

# A chiral quark model for meson electro-production in the S11 partial wave

B. Golli<sup>1</sup> and S. Širca<sup>2</sup>

<sup>1</sup> Faculty of Education, University of Ljubljana and J. Stefan Institute, 1000 Ljubljana, Slovenia

<sup>2</sup> Faculty of Mathematics and Physics, University of Ljubljana and J. Stefan Institute, 1000 Ljubljana, Slovenia

June 2, 2019

**Abstract.** We calculate the meson scattering and electroproduction amplitudes in the S11 partial wave in a coupled-channel approach that incorporates quasi-bound quark-model states. Using the quark wave functions and the quark-meson interaction from the Cloudy Bag Model, we obtain consistent predictions for the partial widths of the  $N(1535)$  and the  $N(1650)$  resonances as well as for the pion, eta and kaon electroproduction amplitudes. Our model suggests that the  $N(1535)$  resonance is dominantly a genuine three-quark state rather than a quasi-bound state of mesons and baryons.

**PACS.** 11.80.Gw, 12.39.Ba, 13.60.Le, 14.20.Gk

## 1 Introduction

In the recent few years there has been a growing interest to understand the nature of the resonances in the second energy region, in particular of the  $N(1440)$  and the two closely lying resonances in the S11 partial wave, the  $N(1535)$  and the  $N(1650)$ . The new experiments on photo and electroproduction of mesons accompanied by the coupled-channel analyses by different groups [1–8] along with analyses of elastic and inelastic scattering data performed mostly before 1995 [9–12] have provided valuable information on the properties of these resonances.

From the theoretical side there have been substantial efforts to understand the peculiar nature of the lightest of the S11 resonances, the  $N(1535)$ , due to its position just above the  $\eta N$  threshold and the large branching ratio to the  $\eta N$  channel. In the quark model this resonance appears as a mixture of two  $\underline{70}$ -plet states with spin 1/2 and 3/2, which can explain the large  $\eta N$  branching ratio of the  $N(1535)$  and the almost complete absence of this decay in the case of its orthogonal partner, the  $N(1650)$  [13]. The mixing originates from the gluon and the meson interaction with quarks, and has been investigated in the constituent quark model [14] and in the bag model [15, 16]. In an alternative picture, this resonance has been explained as a quasi-bound state of mesons and baryons with a strong admixture of the  $K\Lambda$  and  $K\Sigma$  (hidden) channels, in the framework of a potential model [17] and the chiral perturbation theory [18–22]. The scattering amplitudes can be as well reproduced in coupled-channel dynamical models with two genuine quark states for the two lowest S11 wave resonances [23–25] as in models assuming a quasi-bound state of mesons and baryons. However,

in the latter approaches, the calculation of meson photo-production amplitudes [26] shows that an admixture of a genuine state corresponding to the  $N(1535)$  is necessary in order to obtain the appropriate phases for the photo-production amplitudes. This shows that the nature of the  $N(1535)$  is governed by a subtle interplay of quark and meson degrees of freedom which requires further investigations in coupled-channel dynamical models that involve quarks and mesons.

In our previous work we have developed a model that incorporates excited baryons represented as quasi-bound quark-model states into a coupled-channel formalism using the  $K$ -matrix approach [27]. In our method, the meson-baryon and the photon-baryon vertices are determined by the underlying quark model rather than fitted to the experimental data as is the case in phenomenological approaches. We have investigated the P33 and P11 scattering as well as electroproduction amplitudes dominated by the low-lying positive-parity resonances  $\Delta(1232)$ ,  $\Delta(1600)$  and  $N(1440)$  [27, 28].

The extension of the approach to low-lying negative-parity resonances implies the inclusion of new channels involving the  $s$ - and  $d$ -wave pions, the  $\eta$  and the  $\rho$  mesons, and the  $K\Lambda$  channel. The photoproduction of mesons has been studied in a chiral constituent quark model [29–33]. In this approach the widths of the resonances have been either fitted or taken from the PDG while in our approach they are calculated from the quark-model wave functions.

In our previous calculation [27, 28] we have found a good agreement with the experiment for the scattering amplitudes as well as for the electroproduction amplitudes by using a simple chiral quark model, the Cloudy Bag Model (CBM) with the standard choice of parameters that

had been widely adopted in studying the static properties of the nucleon and some low lying resonances.

The aim of this paper is to check whether the same model is able to describe a rather specific situation in the S11 partial wave with two closely lying resonances and a strong admixture of the inelastic channel very close to its threshold. Furthermore, our aim is

(i) to investigate whether the particular form of the quark-meson coupling that works well for the  $p$ -wave pions performs equally well for the  $s$ - and  $d$ -wave pions, and for the other pseudoscalar octet mesons;

(ii) to study the role of the meson cloud which – based on our experience in the P11 and P33 partial waves – is expected to enhance rather substantially the strength of the meson-baryon and photon-baryon vertices with respect to their bare values;

(iii) to examine whether the dominant contribution to the electroexcitation amplitudes originates in the underlying three-quark bound state or is it dynamically generated through the meson cloud.

In the next section we briefly explain how our method can be used to calculate the meson scattering and the electroproduction amplitudes in a unified approach. We generalize the approach of [28] to include the production of mesons other than pions.

In sect. 3 we discuss the results for the scattering amplitudes and concentrate on the  $\eta N$  and  $K\Lambda$  inelastic channels. We investigate the sensitivity of the amplitudes in the resonance region to the relative strength of the quark-pion and the quark- $\eta$  coupling.

In sect. 4 we present the results for the transverse helicity amplitude  $A_{1/2}$  and the scalar helicity amplitude  $S_{1/2}$  for the  $N(1535)$  and the  $N(1650)$  resonances. Finally, we present the results for the  $\gamma N \rightarrow \pi N$  amplitude at the photon point and at  $Q^2 = 1 \text{ (GeV/c)}^2$ , and for photoproduction in the  $\gamma N \rightarrow \eta N$  and  $\gamma N \rightarrow K\Lambda$  channels.

## 2 Basics of the $K$ -matrix approach

We consider a class of chiral quark models in which mesons couple linearly to the quark core:

$$H' = \int dk \sum_{lmt} \left\{ \omega_k a_{lmt}^\dagger(k) a_{lmt}(k) + \left[ V_{lmt}(k) a_{lmt}(k) + V_{lmt}^\dagger(k) a_{lmt}^\dagger(k) \right] \right\}, \quad (1)$$

where  $a_{lmt}^\dagger(k)$  is the creation operator for a meson with angular momentum  $l$ , its third component  $m$ , and isospin  $t$  (absent in the case of  $s$ -waves and isoscalar mesons). Here  $V_{lmt}(k)$  is a general form of the meson source involving the quark operators and is model dependent. In appendix A we give a few examples for  $V_{lmt}(k)$  in the Cloudy Bag Model.

We have shown [27] that in such models the elements of the  $K$  matrix in the basis with good total angular momentum  $J$  and isospin  $T$  take the form:

$$K_{M'B' MB}^{JT} = -\pi \mathcal{N}_{M'B'} \langle \Psi_{JT}^{MB} || V_{M'}(k) || \tilde{\Psi}_{B'} \rangle,$$

$$\mathcal{N}_{MB} = \sqrt{\frac{\omega_M E_B}{k_M W}}, \quad (2)$$

where  $\omega_M$  and  $k_M$  are the energy and momentum of the incoming or outgoing meson,  $E_B$  is the baryon energy and  $W$  is the invariant energy of the meson-baryon system. The channels are also specified by the relative angular momentum of the meson-baryon system and parity. Here  $|\Psi^{MB}\rangle$  is the principal-value state:

$$|\Psi_{JT}^{MB}\rangle = \mathcal{N}_{MB} \left\{ [a^\dagger(k_M) |\tilde{\Psi}_B\rangle]^{JT} + \sum_{\mathcal{R}} c_{\mathcal{R}}^{MB} |\Phi_{\mathcal{R}}\rangle + \sum_{M'B'} \int \frac{dk \chi^{M'B' MB}(k, k_M)}{\omega_k + E_{B'}(k) - W} [a^\dagger(k) |\tilde{\Psi}_{B'}\rangle]^{JT} \right\}. \quad (3)$$

The first term represents the free meson ( $\pi$ ,  $\eta$ ,  $\rho$ ,  $K$ , ...) and the baryon ( $N$ ,  $\Delta$ ,  $\Lambda$ , ...) and defines the channel, the next term is the sum over *bare* three-quark states  $\Phi_{\mathcal{R}}$  involving different excitations of the quark core, the third term introduces meson clouds around different isobars,  $E(k)$  is the energy of the recoiled baryon. In our approach we assume the commonly used picture in which the two-pion decay proceeds either through an unstable meson ( $\rho$ -meson,  $\sigma$ -meson, ...) or through a baryon resonance ( $\Delta(1232)$ ,  $N(1440)$  ...). In such a case the state  $\Psi^{MB}$  depends on the invariant mass of the subsystem (either  $\pi\pi$  or  $\pi N$ ) and the sum over  $M'B'$  in (3) also implies the integration over the invariant mass. The state  $\tilde{\Psi}_B$  is the asymptotic state of the incoming or outgoing baryon; in the case when it corresponds to an unstable baryon, it depends on the invariant mass of the  $\pi N$  subsystem,  $M_B$ , and is normalized as  $\langle \tilde{\Psi}_B(M'_B) | \tilde{\Psi}_B(M_B) \rangle = \delta(M'_B - M_B)$ , where  $M_B$  is the invariant mass of the  $\pi N$  subsystem. The meson amplitudes  $\chi^{M'B' MB}(k, k_M)$  are proportional to the half off-shell matrix elements of the  $K$ -matrix

$$K_{M'B' MB}(k, k_M) = \pi \mathcal{N}_{M'B'} \mathcal{N}_{MB} \chi^{M'B' MB}(k, k_M) \quad (4)$$

and obey an equation of the Lippmann-Schwinger type:

$$\begin{aligned} \chi^{M'B' MB}(k, k_M) = & - \sum_{\mathcal{R}} c_{\mathcal{R}}^{MB} V_{B'\mathcal{R}}^{M'}(k) \\ & + \mathcal{K}^{M'B' MB}(k, k_M) \\ & + \sum_{M''B''} \int dk' \frac{\mathcal{K}^{M'B' M''B''}(k, k') \chi^{M''B'' MB}(k', k_M)}{\omega'_k + E_{B''}(k') - W}, \end{aligned} \quad (5)$$

where

$$\mathcal{K}^{M'B' MB}(k, k') = \sum_{B''} f_{BB''}^{B'} \frac{\tilde{V}_{B''B'}^{M'}(k') \tilde{V}_{B''B}^M(k)}{\omega_k + \omega'_k + E_{B''}(k) - W}, \quad (6)$$

$$f_{AB}^C = \sqrt{(2J_A+1)(2J_B+1)(2T_A+1)(2T_B+1)} \times W(1J_A J_B 1; J_C, J) W(1T_A T_B 1; T_C, T). \quad (7)$$

The coefficients  $c_{\mathcal{R}}^{MB}$  obey the equation

$$(W - M_{\mathcal{R}}^{(0)})c_{\mathcal{R}}^{MB} = V_{B\mathcal{R}}^M(k_M) + \sum_{M'B'} \int dk \frac{\chi^{M'B' MB}(k, k_M) V_{B'\mathcal{R}}^{M'}(k)}{\omega_k + E_{B'}(k) - W}. \quad (8)$$

Here  $V_{B\mathcal{R}}^M(k)$  are the matrix elements of the quark-meson interaction between the baryon state  $B$  and the bare three-quark state  $\Phi_{\mathcal{R}}$ , and  $M_{\mathcal{R}}^{(0)}$  is the energy of the bare state. Solving the coupled system of equations (5) and (8) using a separable approximation for the kernels (6) (see [27]), the resulting amplitudes take the form

$$\chi^{M'B' MB}(k, k_M) = - \sum_{\mathcal{R}} \tilde{c}_{\mathcal{R}}^{MB} \tilde{V}_{B'\mathcal{R}}^{M'}(k) + \mathcal{D}^{M'B' MB}(k, k_M), \quad (9)$$

where the first term represents the contribution of various resonances while  $\mathcal{D}^{M'B' MB}(k)$  originates in the non-resonant background processes. Here

$$\tilde{c}_{\mathcal{R}}^{MB} = \frac{\tilde{V}_{B\mathcal{R}}^M}{Z_{\mathcal{R}}(W)(W - M_{\mathcal{R}})}, \quad (10)$$

$\tilde{V}_{B\mathcal{R}}^M$  is the dressed matrix element of the quark-meson interaction between the resonant state and the baryon state in the channel  $MB$ , and  $Z_{\mathcal{R}}$  is the wave-function normalization. The physical resonant state  $\mathcal{R}$  is a superposition of the dressed states built around the bare three-quark states  $\Phi_{\mathcal{R}}$ .

The  $T$  matrix is finally obtained by solving the Heitler's equation

$$T = K + iTK. \quad (11)$$

The method can be extended in a straightforward manner to the calculation of electroproduction amplitudes by including the  $\gamma N$  channel. As we have shown in [28] the electroproduction amplitudes for the pion can be split into the resonant part and the background part. This splitting can be generalized to electroproduction of other mesons. The resonant part reads

$$\mathcal{M}_{\gamma NMB}^{(\text{res})} = \sqrt{\frac{\omega_{\gamma} E_N^{\gamma}}{\omega_M E_B}} \frac{\zeta}{\pi \tilde{V}_{B N^*}} \langle \Psi_{N^*}^{(\text{res})}(W) | \tilde{V}_{\gamma} | \Psi_N \rangle T_{MB MB}, \quad (12)$$

where  $\tilde{V}_{\gamma}(\mu, \mathbf{k}_{\gamma})$  is the interaction of the photon with the electromagnetic current which contains quark and pion contributions,

$$\mathbf{j}_{EM}(\mathbf{r}) = \bar{\psi} \boldsymbol{\gamma} \left( \frac{1}{6} + \frac{1}{2} \tau_0 \right) \psi + i \sum_t t \pi_t(\mathbf{r}) \nabla \pi_{-t}(\mathbf{r}),$$

$T_{MB MB}$  is the meson-baryon scattering amplitude, and  $\zeta$  is the spin-isospin factor depending on the considered multipole and the spin and isospin of the outgoing hadrons. The state  $\Psi_{N^*}^{(\text{res})}$  is obtained from (3) by keeping only the linear combination of  $\mathcal{R}$  representing  $N^*$  in the sum over

$\mathcal{R}$  and the corresponding term in the sum in (9). The expression  $\langle \Psi_{N^*}^{(\text{res})}(W) | \tilde{V}_{\gamma} | \Psi_N \rangle = A_{\gamma N \rightarrow N^*}$  is the electroexcitation amplitude of the chosen resonance  $N^*$ .

The background part of the electroproduction amplitude satisfies

$$\mathcal{M}_{MB}^{(\text{bkg})} = \mathcal{M}_{MB}^{K(\text{bkg})} + i \sum_{M'B'} T_{MB M'B'} \mathcal{M}_{M'B'}^{K(\text{bkg})}. \quad (13)$$

Here  $\mathcal{M}_{M'B'}^{K(\text{bkg})}$  is the expectation value of the electromagnetic interaction between the nucleon and the channel state  $\Psi_{M'B'}^{JT}$  (3) without the terms pertinent to the resonant state  $N^*$ . It contains the contribution from the other resonances, from the scattering background (the  $\mathcal{D}$  term in (9)), and from the first term in (3). The latter term, representing the unperturbed meson, is responsible for the terms corresponding to the  $t$ - and  $u$ -channel processes.

### 3 The S11 scattering amplitudes

We have used the Cloudy Bag Model to describe the quark wave-functions and quark-meson coupling; the details are given in appendix A. The parameters of the model are the bag radius and the strength of the quark-pion coupling  $f_{\pi}$  (corresponding to the pion decay constant) set to  $f_{\pi} = 76$  MeV which reproduces the experimental value of the  $\pi NN$  coupling constant. For the bag radius we use  $R_{\text{bag}} = 0.83$  fm yielding best results for the ground state properties and also for the scattering and electroproduction amplitudes in the P11 and P33 partial waves. Further free parameters of the present calculations are the masses of the bare three-quark states and the mixing angle  $\vartheta_S$  discussed below.

To calculate the scattering and electroproduction amplitudes in the S11 partial wave we have included the  $\pi N$ ,  $\pi \Delta(1232)$ ,  $\pi N(1440)$ ,  $\rho N$ , and  $KA(1116)$  channels, and the  $N(1535)$  and  $N(1650)$  resonances. The quark-model wave-functions for the negative-parity states in the  $j$ - $j$  coupling scheme have been taken from [16]:

$$\Phi_{\mathcal{R}} = c_A^{\mathcal{R}} |(1s)^2(1p_{3/2})^1\rangle + c_P^{\mathcal{R}} |(1s)^2(1p_{1/2})^1\rangle_1 + c_{P'}^{\mathcal{R}} |(1s)^2(1p_{1/2})^1\rangle_2, \quad (14)$$

where the mixing coefficients  $c_A^{\mathcal{R}}$ ,  $c_P^{\mathcal{R}}$ , and  $c_{P'}^{\mathcal{R}}$  are expressed in terms of the mixing angle  $\vartheta_s$  between the spin-1/2 and spin-3/2 three-quark configurations. They are given by

$$\begin{aligned} c_A^1 &= -\frac{1}{3}(2 \cos \vartheta_s + \sin \vartheta_s), \\ c_P^1 &= \frac{\sqrt{2}}{6}(\cos \vartheta_s - 4 \sin \vartheta_s), \quad c_{P'}^1 = \frac{\sqrt{2}}{2} \cos \vartheta_s, \\ c_A^2 &= \frac{1}{3}(\cos \vartheta_s - 2 \sin \vartheta_s), \\ c_P^2 &= \frac{\sqrt{2}}{6}(\sin \vartheta_s + 4 \cos \vartheta_s), \quad c_{P'}^2 = \frac{\sqrt{2}}{2} \sin \vartheta_s. \end{aligned}$$

In this coupling scheme the spurious translational state belonging to the SU(6) spin-flavour  $\underline{56}$ -plet is projected out.

The mixing is a consequence of the gluon and the meson interactions; since the quark-gluon interaction is not included in the model, the mixing angle due to the gluons is taken as a free parameter independent of  $W$ . In the energy region of the  $N(1535)$  and  $N(1650)$  resonances we obtain the best results using  $\vartheta_s = -34^\circ$  for the bare states; after taking into account the mixing due to the meson loops, the value of the mixing angle reaches  $-30^\circ$  in agreement with the phenomenological analysis [13]. The results, however, do not depend strongly on the mixing angle, and deviations in  $\vartheta_s$  of the order  $\approx 5^\circ$  lead to similar results. The poles of the  $K$  matrix are at 1537 MeV and 1690 MeV, and almost exactly coincide with zero crossings of the real parts of the  $\eta N$  and  $\pi N$  amplitudes, respectively. The corresponding masses of the bare three-quark states are 1760 MeV and 1810 MeV, which are close to the bare values used in [24].

Solving the equation for the meson amplitudes (5) we have taken into account the  $s$ - and  $p$ -wave pions, the  $s$ -wave  $\eta$  mesons, and the following intermediates states:  $N$ ,  $N(1440)P_{11}$ ,  $\Delta(1232)P_{33}$ ,  $\Delta(1600)P_{33}$ ,  $N(1535)S_{11}$ ,  $N(1650)S_{11}$ ,  $N(1520)D_{13}$ ,  $N(1700)D_{13}$ ,  $\Delta(1630)D_{31}$ ,  $\Delta(1700)D_{33}$ . All baryon-meson couplings have been calculated in the Cloudy Bag Model while the standard PDG values [34] have been used for the masses of the intermediate states. The contributions from the  $d$ -wave pions and  $J = \frac{5}{2}$  resonances as well as from the  $s$ -wave kaons turn out to be small.

Res.	$\Gamma_{\text{tot}}$	$\Gamma_i/\Gamma_{\text{tot}}$					
	[MeV]	$\pi N$	$\eta N$	$\pi\Delta$	$K\Lambda$	$\rho_1 N$	$\pi R$
$N(1535)$	110	0.37	0.60	0.01	-	0.02	0
$N(1535)'$	160	0.29	0.69	0.01	-	0.01	0
Exp.	125 - 175	0.35 - 0.55	0.53	0.01	-	0.02	0
$N(1650)$	174	0.61	0	0.20	0.10	0.04	0.04
$N(1650)'$	152	0.71	0	0.08	0.11	0.05	0.04
Exp.	150 - 180	0.60 - 0.95	0.02	0.02	0.03	0.01	0.03

**Table 1.** The total and the partial widths for the  $N(1535)$  and the  $N(1650)$  resonance at the  $K$ -matrix pole (1537 MeV and 1690 MeV, respectively). Here  $N(1535)'$  stands for the results using the value  $f_\eta = f_\pi$  (instead of  $f_\eta = 1.2 f_\pi$ ), and  $N(1650)'$  for the results using the value of the  $d$ -wave  $\pi\Delta$  coupling reduced by a factor of 0.60 compared to the quark-model prediction;  $\pi R$  means the  $\pi N(1440)$  channel. The experimental values are from [34].

The results for pion-induced meson production are displayed in table 1 and figs. 1–3. In the vicinity of the lower ( $N(1535)$ ) resonance, just above the  $\eta$  threshold, the elastic and inelastic amplitudes are strongly influenced by the  $s$ -wave  $\eta N$  channel. In the energy region of the upper resonance ( $N(1650)$ ), additional channels open or become more important. We have considered the following ad-

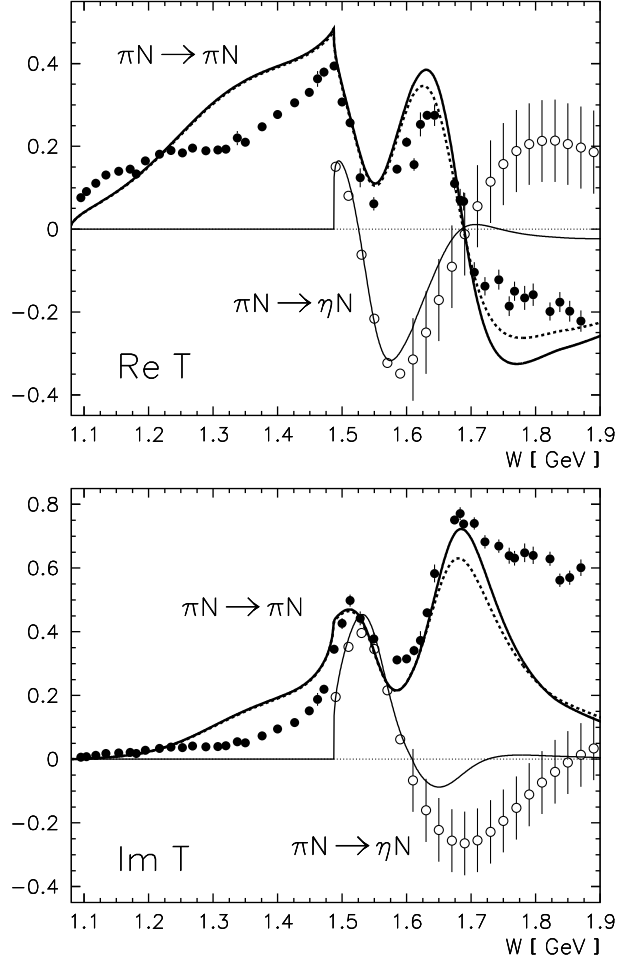


**Fig. 1.** The real and the imaginary part of the scattering  $T$  matrix for the S11 partial wave. The thick solid and dashed lines correspond to the elastic channel and the thin solid lines to the  $\pi N \rightarrow \eta N$  channel. The solid lines are obtained by using the reduced value of the  $d$ -wave  $\pi\Delta$  coupling while the dashed lines correspond to the unmodified quark-model values for the baryon-meson couplings. The data points for the elastic channel (full circles) are from the SAID  $\pi N \rightarrow \pi N$  partial-wave analysis [4], those for the inelastic one (open circles) are from [35].

ditional channels: the  $\pi\Delta$  channel with  $l = 2$ , the  $K\Lambda$  channel with  $l = 0$ , two channels involving the  $\rho$  meson with  $l = 0$  ( $\rho_1 N$ ) and  $l = 2$  ( $\rho_3 N$ ), and the  $\pi N(1440)$  channel with  $l = 0$ . Using the quark-model values for the quark-meson coupling as introduced in appendix A we obtain a good agreement between the model prediction and the experimental analysis for the lower resonance; for the upper resonance the agreement is worse. Though the extraction of the experimental points is less reliable and differs considerably between different authors, the results clearly indicate that the strength of the  $\pi\Delta$  ( $d$ -wave) vertex is overestimated in our model (table 1). Multiplying the strength of the  $\pi\Delta$  vertex by 0.6 yields a better agree-

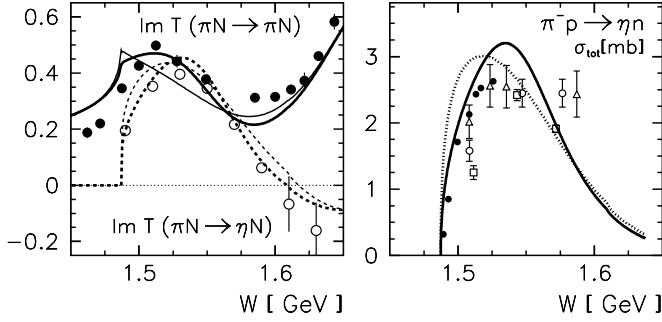


**Fig. 2.** Left panel: the imaginary part of the  $T$  matrix for elastic scattering (solid lines) and for the  $\eta N$  channel (dashed lines) in the region of the  $N(1535)$ . The thick lines correspond to  $f_\eta = 1.2 f_\pi$ , the thin lines to  $f_\eta = f_\pi$ . Right panel: the (dominant) S11 contribution to the total cross-section for the  $\pi^- p \rightarrow \eta n$  reaction using  $f_\eta = 1.2 f_\pi$  (solid line) and  $f_\eta = f_\pi$  (dotted line). Experimental data in the left panel: see fig. 1. Experimental data in the right panel are from [36] (open triangles), [37] (open circles), [38] (open squares), and [39] (filled circles).

ment with the data (fig. 3) and improves the agreement with the imaginary part of the elastic  $T$  matrix (fig. 1).

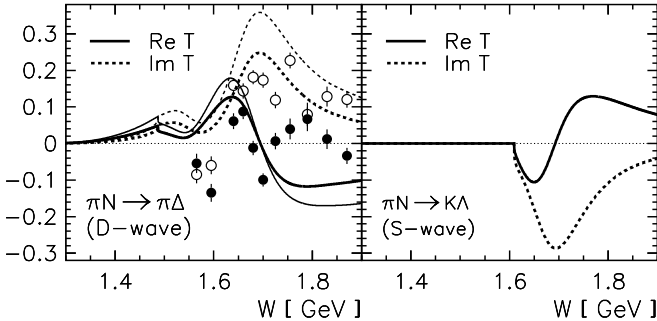


**Fig. 3.** The real and the imaginary part of the  $T$  matrix for the  $\pi N \rightarrow \pi \Delta$  (left panel) and for the  $\pi N \rightarrow K \Lambda$  channel (right panel) in the S11 partial wave. The thick lines are obtained by using the reduced value of the  $d$ -wave  $\pi \Delta$  coupling while the thin lines correspond to the unmodified quark-model values for the baryon-meson couplings. The experimental points are from [12].

The behaviour of the imaginary part of the  $\pi N$  amplitude is very sensitive to the value of  $f_\eta$ ; for our standard choice  $f_\eta = 1.2 f_\pi$  we get a typical resonant peak at around 1510 MeV while for  $f_\eta = f_\pi$  (corresponding to a stronger quark- $\eta$  coupling) this peak disappears and we end up with a cusp at the  $\eta N$  threshold (fig. 2). The effect of reducing  $f_\eta$  also strongly influences the total width of the resonances and the  $\pi N$  branching ratio (table 1). This effect is not so pronounced in the case of the  $\eta N$  amplitudes. The comparison of the calculated total cross section for the reaction  $\pi^- p \rightarrow \eta n$  which is dominated by the  $\eta N$  channel up to  $W \sim 1650$  MeV [40] with the recent

precise measurement [39] seems to favour the higher value of  $f_\pi$  (fig. 2, right panel).

The bag radius determines the overall strength of the quark-meson interaction and an effective momentum cut-off which for the  $s$ -wave mesons and  $R_{\text{bag}} = 0.83$  fm corresponds to  $\Lambda = 510$  MeV/c. Taking a larger radius,  $R_{\text{bag}} = 0.90$  fm, the widths of the resonances are reduced by  $\sim 35\%$ , but the behaviour of the elastic amplitude improves in the region below the  $\eta N$  threshold. Decreasing the bag radius the widths increase and at the same time the mass of the bare  $N(1535)$  increases while that of the  $N(1650)$  decreases. Below a certain critical  $R_{\text{bag}}$  no solution exists for the bare masses if the positions of the  $K$ -matrix poles remain fixed; this might be an indication that the picture with two genuine three-quark states breaks down and quark-meson couplings become sufficiently strong to support a quasi-bound state of mesons and baryons.

## 4 The meson electroproduction amplitudes

In the S11 partial wave, electroproduction of mesons is dominated by the  $E_{0+}$  and  $S_{0+}$  amplitudes. The corresponding  $E1$  and  $C1$  multipole operators have the familiar forms

$$V_\gamma^{E1} = \frac{ie\sqrt{3\pi}\mu}{\sqrt{2\omega_\gamma}k_\gamma} \int d\mathbf{r} \left[ \mathbf{j}_{EM}(\mathbf{r}) \cdot \nabla \left( Y_{1\mu}(\hat{r}) \frac{\partial}{\partial r} r j_1(k_\gamma r) \right) + k_\gamma^2 \mathbf{r} \cdot \mathbf{j}_{EM}(\mathbf{r}) j_1(k_\gamma r) Y_{1\mu}(\hat{r}) \right] \quad (15)$$

and

$$V_\gamma^{C1} = \frac{e\sqrt{12\pi}}{\sqrt{2\omega_\gamma}} \int d\mathbf{r} j_1(k_\gamma r) Y_{10}(\hat{r}) \rho_{EM}(\mathbf{r}). \quad (16)$$

The relations between the helicity and the pion electroproduction amplitudes are the same as for the  $M1$  multipole and are given in [28]. For  $\zeta$  in (12) we have  $\zeta_E = \sqrt{1/12}$  for the transverse and  $\zeta_S = \sqrt{1/6}$  for the scalar amplitude, and  $\zeta_E = \sqrt{1/2}$  and  $\zeta_S = 1$  for the  $\eta N$  and  $K \Lambda$  amplitudes.

The helicity amplitudes are displayed in fig. 4 and fig. 5. The values for the transverse amplitudes are well reproduced at the photon point and in the low- $Q^2$  region. For  $Q^2 > 1.5$  (GeV/c) $^2$  the calculated amplitudes become smaller compared to the data indicating that our simple quark model is not able to reproduce the short range behaviour of the quark wave-function in the nucleon. The pion cloud contributes considerably in the region of low  $Q^2$ . In the  $N(1535)$  case, the pion contribution and the vertex corrections improve the agreement with the data. For the scalar amplitude this contribution is however not sufficient to partially cancel the large quark part. In the transverse amplitude for the  $N(1650)$ , the strength of the pion cloud contributions is about half of the quark part, while in the scalar case, the pion and quark parts largely

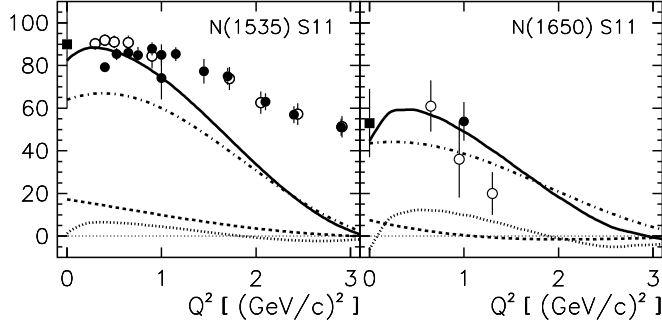


**Fig. 4.** The proton transverse helicity amplitudes (solid lines) for the  $N(1535)$  (left panel) and for the  $N(1650)$  (right panel) evaluated at the pole of the  $K$  matrix, in units of  $10^{-3} \text{ GeV}^{-1/2}$ . The dashed-dotted lines correspond to the quark contribution, the dotted lines to the pion contribution and the dashed lines to vertex corrections. Experimental data are from the PDG [34] (filled squares at  $Q^2 = 0$ ), MAID [2,41] (filled circles), and analyses of CLAS data [1,42] (open circles).

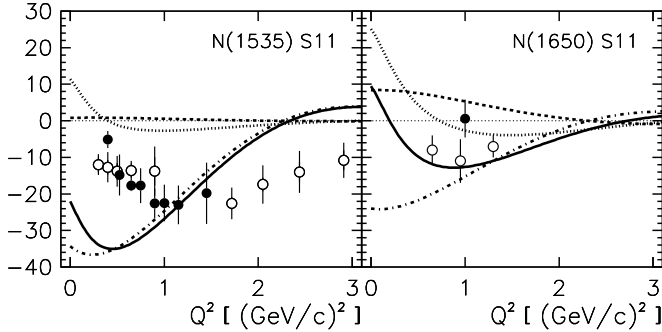


**Fig. 5.** The proton scalar helicity amplitudes for the  $N(1535)$  and  $N(1650)$  resonances. Notation as in fig. 4.

cancel at low  $Q^2$  and bring the sum into a better agreement with the data compared to the  $N(1535)$  case.

The  $E_{0+}$  electroproduction amplitude for  $\gamma p \rightarrow \pi N$  is displayed in fig. 6 and fig. 7 for  $Q^2 = 0$  and  $Q^2 = 1 \text{ (GeV/c)}^2$ , and for  $\gamma n \rightarrow \pi N$  at  $Q^2 = 0$  in fig. 7. Since the model reproduces well the transverse helicity amplitudes in the resonance region, the electroproduction amplitudes also agree well with the phenomenologically determined amplitudes. The good agreement extends also into the region below the resonance where the dominant contribution arises from the pion  $t$ -channel. Our model, however, fails to reproduce the threshold behaviour of the  $E_{0+}$  amplitudes since it assumes the pseudoscalar pion-quark coupling and hence does not contain the Kroll-Ruderman term. (This term can be *ad hoc* included in the model but since we are primarily interested in the resonance region we have not considered such a possibility.) The  $S_{0+}$  scalar amplitude for  $\gamma p \rightarrow \pi N$  is shown in fig. 8. Since our model overestimates the size of the scalar helicity amplitude at the photon point it also disagrees with the phenomenologically determined amplitudes in the resonance

region for  $Q^2 = 0$  but yields a consistent prediction at  $Q^2 \sim 1 \text{ (GeV/c)}^2$ .

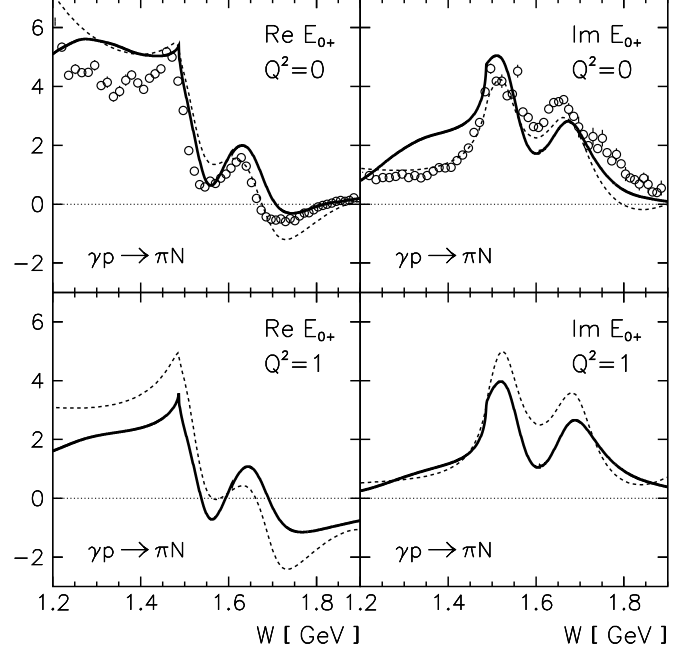


**Fig. 6.** The transverse amplitude  $E_{0+}$  for  $\gamma p \rightarrow \pi N$  at  $Q^2 = 0$  (upper panel) and  $Q^2 = 1 \text{ (GeV/c)}^2$  (lower panel) in units of  $10^{-3} m_\pi^{-1}$ . Dashed lines correspond to the MAID analysis [2], the experimental data are from [43].

The results for  $\eta$  photoproduction are compared to the phenomenological prediction for the  $E_{0+}$  amplitude and the total cross section in fig. 9. The results almost entirely depend on the properties of the lower  $N(1535)$  resonance and the threshold behaviour of the  $\eta N$  amplitude but very little on the background processes. Our standard choice  $f_\eta = 1.2 f_\pi$  yields somewhat too narrow amplitudes; in contrast to the  $\pi N \rightarrow \eta N$  process, the choice  $f_\eta = f_\pi$  leads to a better agreement. The good overall agreement with the data for  $\eta$  production strongly supports our conjecture about the dominance of the genuine three-quark configuration in the  $N(1535)$  state.

The situation is less clear in the  $K\Lambda$  channel displayed in fig. 10 since different analyses yield rather inconsistent results, in particular for the phase of the  $E_{0+}$  amplitude. Our prediction for the absolute value is consistent with the recent compilation of various analyses by Sandorfi and coauthors [44]. The real and the imaginary parts of the  $E_{0+}$  amplitude agree with the analysis of the MAID group except in the region of the  $N(1650)$  resonance; the discrepancy can probably be attributed to the higher position of the pole of the  $K$  matrix which is at  $W = 1690 \text{ MeV}$  in our calculation. While the results for the inelastic scattering amplitudes (table 1 and fig. 3) indicate that the strength of the  $K\Lambda$  coupling is overestimated in our model, the results for photoproduction (fig. 10) show that our value for

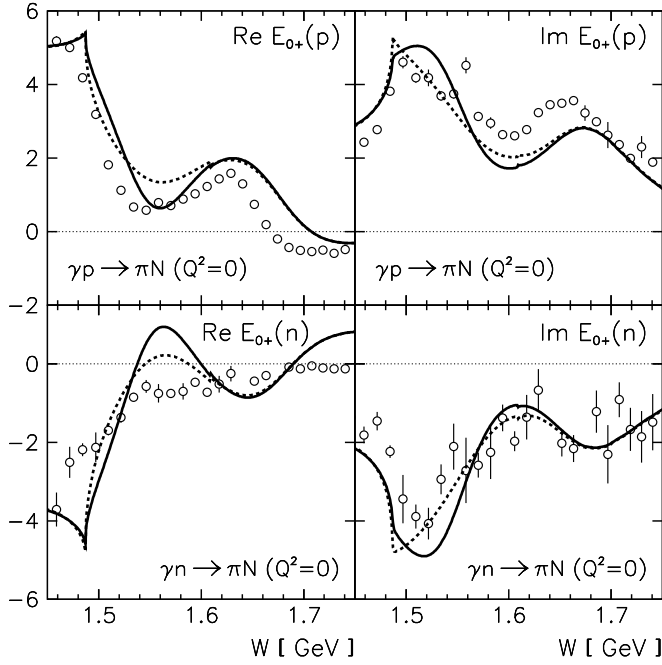


**Fig. 7.** The transverse pion photoproduction amplitudes  $E_{0+}$  on the proton (upper panels, zoom-in of fig. 6) and on the neutron (lower panels) in units  $10^{-3} m_{\pi}^{-1}$ . The solid lines correspond to  $f_{\eta} = 1.2 f_{\pi}$ , the dashed lines to  $f_{\eta} = f_{\pi}$ . The experimental data are from [43].

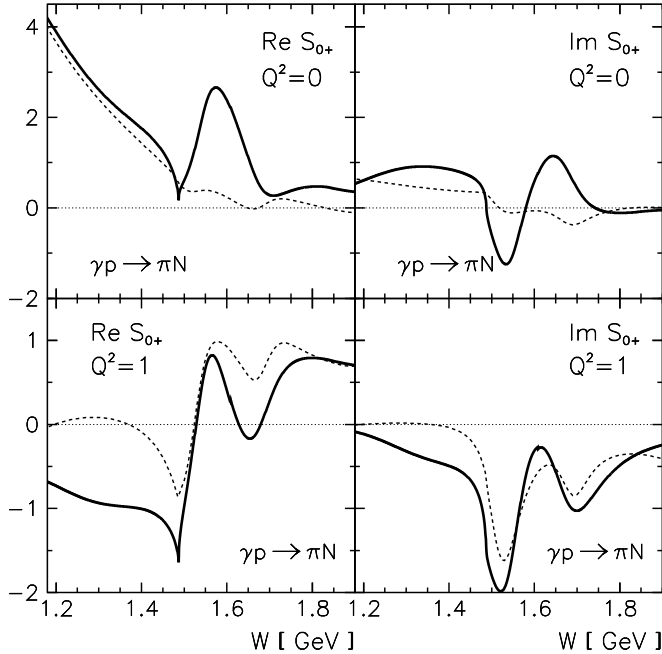


**Fig. 8.** The scalar pion production amplitude  $S_{0+}$ . Notation as in fig. 6.

this coupling is not inconsistent with the phenomenological analyses.

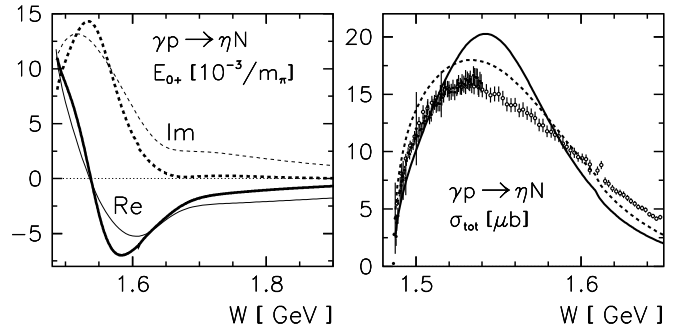


**Fig. 9.** Eta photoproduction on the proton. Left panel: real and imaginary parts of the  $E_{0+}$  multipole; our result (thick lines); EtaMAID [45] (thin lines). Right panel: total cross-section; our result ( $f_{\eta} = 1.20 f_{\pi}$ : solid line,  $f_{\eta} = f_{\pi}$ : dashed line). The experimental data are from [46] and [47].

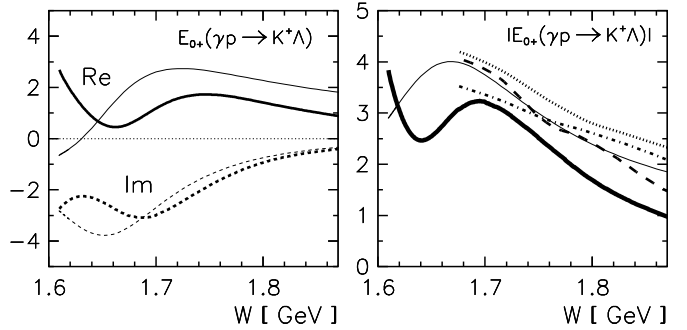


**Fig. 10.** The transverse  $K^+$ -production amplitude  $E_{0+}$ . Left panel: real and imaginary parts; our result (thick lines); KaonMAID [8] (thin lines). Right panel: absolute value of the amplitude; our result (thick solid line); KaonMAID (thin solid line); SAID [48] (dotted line); Bonn-Gatchina [3] (dot-dashed line), JSLT [23] (long-dashed line).

## 5 Conclusions

Using our method based on the coupled-channel formalism incorporating quark-model quasi-bound states, and the Cloudy Bag Model to describe the quark states and the coupling to the mesons, we have been able to reproduce the main features of  $\pi$ - and  $\gamma$ -induced production of pions,  $\eta$  mesons, and kaons. We have used the same model parameters as in the case of the positive-parity resonances, adding only the mixing parameter between the two bare-quark states corresponding to  $N(1535)$  and  $N(1650)$ , and their bare masses. We have not attempted to add further adjustable parameters in order to obtain a perfect fit to available data, being aware of the limitations of the model which, in general, is able to reproduce different observables pertinent to the ground state and the excited states within  $\sim 20\%$ .

The role of the meson cloud turns out to be important in two aspects: it enhances the bare baryon-meson coupling and improves the behaviour of the helicity amplitudes in the region of low  $Q^2$ . The enhancement is however not so strong as in the case of the positive-parity

resonances and the electroexcitation amplitudes are dominated by the quark contribution. The enhancement does not lead to a formation of meson-baryon quasi-bound states as predicted by some models based on the Weinberg-Tomozawa type of meson-baryon interaction. The critical parameter to distinguish between the two mechanisms of resonance formation can be related to the effective momentum cut-off which in our case corresponds to a rather low value of  $\sim 500$  MeV/c.

The couplings of the resonances to different inelastic channels are reasonably well reproduced particularly in the  $\eta N$  channel. At present, the experimental data are insufficient to support a reliable multipole analysis of the  $K\Lambda$  photoproduction channel [48], and there is a large spread of predictions for the  $E_{0+}$  multipole. Our calculation of this channel does not appear to be in conflict with any of them. We therefore conclude that our assumption about the form of the quark interaction with the pseudoscalar octet mesons is sensible. The  $d$ -wave pion coupling to  $\Delta(1232)$  turns out to be overestimated; for  $\rho N$  channels the available data do not allow us to draw more definitive conclusions.

The authors would like to express their thanks for a helpful discussion with M. Döring regarding the  $K\Lambda$  channel. One of the authors (B. G.) would like to acknowledge the hospitality he enjoyed during a visit to the University of Coimbra and stimulating discussions with M. Fiolhais, L. Alvarez-Ruso and P. Alberto.

## A The Cloudy Bag Model meson-quark vertices

The vertices  $V_{lmt}(k)$  in (1) are evaluated in the Cloudy Bag Model assuming that one of the three quarks is excited from the  $1s$  state to the  $1p_j$  state with the total angular momentum  $j$  either  $1/2$  or  $3/2$ . The relevant quark bispinors in the  $j m_j$  basis are

$$\begin{aligned}\psi_s(\mathbf{r}) &= \frac{N_s}{\sqrt{4\pi} j_0(\omega_s)} \begin{pmatrix} -i j_0(\omega_s r/R) \\ \boldsymbol{\sigma} \cdot \hat{\mathbf{r}} j_1(\omega_s r/R) \end{pmatrix} \chi_{m_j}, \\ \psi_{p_{1/2}}(\mathbf{r}) &= \frac{N_{p_{1/2}}}{\sqrt{4\pi} j_0(\omega_{p_{1/2}})} \begin{pmatrix} i j_1(\omega_{p_{1/2}} r/R) \boldsymbol{\sigma} \cdot \hat{\mathbf{r}} \\ j_0(\omega_{p_{1/2}} r/R) \end{pmatrix} \chi_{m_j}, \\ \psi_{p_{3/2}}(\mathbf{r}) &= \frac{N_{p_{3/2}}}{\sqrt{6\pi} j_1(\omega_{p_{3/2}})} \begin{pmatrix} -i j_1(\omega_{p_{3/2}} r/R) \\ \boldsymbol{\sigma} \cdot \hat{\mathbf{r}} j_2(\omega_{p_{3/2}} r/R) \end{pmatrix} \\ &\quad \times \sum_{m_s m} \chi_{m_s} \hat{r}_m C_{\frac{1}{2} m_s 1 m}^{\frac{3}{2} m_j}.\end{aligned}$$

Here  $\chi_m$  is the spinor for spin  $\frac{1}{2}$ ,  $R$  is the bag radius,  $\omega_s = 2.043$ ,  $\omega_{p_{1/2}} = 3.811$ ,  $\omega_{p_{3/2}} = 3.204$ , and

$$\begin{aligned}N_s^2 &= \frac{\omega_s}{2R^3(\omega_s - 1)}, & N_{p_{1/2}}^2 &= \frac{\omega_{p_{1/2}}}{2R^3(\omega_{p_{1/2}} + 1)}, \\ N_{p_{3/2}}^2 &= \frac{9\omega_{p_{3/2}}}{4R^3(\omega_{p_{3/2}} - 2)}.\end{aligned}$$

For the *quark pion coupling* we obtain

$$\begin{aligned}V_{l=0,t}^\pi(k) &= \frac{1}{2f_\pi} \sqrt{\frac{\omega_{p_{1/2}}\omega_s}{(\omega_{p_{1/2}} + 1)(\omega_s - 1)}} \frac{1}{2\pi} \frac{k^2}{\sqrt{\omega_k}} \frac{j_0(kR)}{kR} \\ &\quad \times \sum_{i=1}^3 \tau_t(i) \mathcal{P}_{sp}(i), \\ V_{1mt}^\pi(k) &= \frac{1}{2f_\pi} \frac{\omega_s}{(\omega_s - 1)} \frac{1}{2\pi} \frac{1}{\sqrt{3}} \frac{k^2}{\sqrt{\omega_k}} \frac{j_1(kR)}{kR} \sum_{i=1}^3 \tau_t(i) \\ &\quad \times \left( \sigma_m(i) + r_{p_{1/2}} S_{1m}^{[\frac{1}{2}]}(i) + r_{p_{3/2}} S_{1m}^{[\frac{3}{2}]}(i) \right), \\ V_{2mt}^\pi(k) &= \frac{1}{2f_\pi} \sqrt{\frac{\omega_{p_{3/2}}\omega_s}{(\omega_{p_{3/2}} - 2)(\omega_s - 1)}} \frac{\sqrt{2}}{2\pi} \frac{k^2}{\sqrt{\omega_k}} \frac{j_2(kR)}{kR} \\ &\quad \times \sum_{i=1}^3 \tau_t(i) \Sigma_{2m}^{[\frac{1}{2}, \frac{3}{2}]}(i).\end{aligned}$$

Here

$$\begin{aligned}\mathcal{P}_{sp} &= \sum_{m_j} |sm_j\rangle \langle p_{1/2} m_j|, \\ S_{1m}^{[\frac{1}{2}]} &= \sqrt{3} \sum_{m_j m'_j} C_{\frac{1}{2} m'_j 1 m}^{\frac{1}{2} m_j} |p_{1/2} m_j\rangle \langle p_{1/2} m'_j|, \\ \Sigma_{2m}^{[\frac{1}{2}, \frac{3}{2}]} &= \sum_{m_s m_j} C_{\frac{3}{2} m'_j 2 m}^{\frac{1}{2} m_s} |sm_s\rangle \langle p_{3/2} m_j|, \\ S_{1m}^{[\frac{3}{2}]} &= \frac{\sqrt{15}}{2} \sum_{m_j m'_j} C_{\frac{3}{2} m'_j 1 m}^{\frac{3}{2} m_j} |p_{3/2} m_j\rangle \langle p_{3/2} m'_j|,\end{aligned}\quad (17)$$

and

$$r_{p_{1/2}} = \frac{\omega_{p_{1/2}}(\omega_s - 1)}{\omega_s(\omega_{p_{1/2}} + 1)}, \quad r_{p_{3/2}} = \frac{2\omega_{p_{3/2}}(\omega_s - 1)}{5\omega_s(\omega_{p_{3/2}} - 2)}.$$

For the  $s$ -wave  $\eta$  and  $K$  mesons we assume the flavour SU(3) symmetry yielding

$$\begin{aligned}V^\eta(k) &= \frac{1}{2f_\pi} \sqrt{\frac{\omega_{p_{1/2}}\omega_s}{(\omega_{p_{1/2}} + 1)(\omega_s - 1)}} \frac{1}{2\pi} \frac{k^2}{\sqrt{\omega_k}} \frac{j_0(kR)}{kR} \\ &\quad \times \sum_{i=1}^3 \lambda_8(i) \mathcal{P}_{sp}(i), \\ V_t^K(k) &= \frac{1}{2f_K} \sqrt{\frac{\omega_{p_{1/2}}\omega_s}{(\omega_{p_{1/2}} + 1)(\omega_s - 1)}} \frac{1}{2\pi} \frac{k^2}{\sqrt{\omega_k}} \frac{j_0(kR)}{kR} \\ &\quad \times \sum_{i=1}^3 (V_t(i) + U_t(i)) \mathcal{P}_{sp}(i),\end{aligned}$$

with  $t = \pm \frac{1}{2}$ ,  $V_{\pm t} = (\lambda_4 \pm i\lambda_5)/\sqrt{2}$ ,  $U_{\pm t} = (\lambda_6 \pm i\lambda_7)/\sqrt{2}$ ,  $f_\eta = 1.20 f_\pi$  [49], and  $f_K = 1.20 f_\pi$  [34].

For the coupling of negative parity states to  $\rho N$ , the dominant contribution is expected to arise from the transverse  $\rho$ -mesons with the total  $J = 1$  and the orbital angular momentum of the  $\rho N$  system equal to either 0 or 2.



Assuming that the  $\rho$  meson couples to the quarks only on the bag surface [50] in the form  $\gamma^\mu \rho_\mu$ , we find (note that  $m$  in (1) and below refers to the total angular momentum rather than to the orbital one):

$$V_{l=0mt}^\rho(k) = \frac{1}{2f_\rho} \sqrt{\frac{\omega_s}{(\omega_s - 1)}} \frac{1}{2\pi} \frac{k^2}{\sqrt{\omega_k}} \frac{j_0(kR)}{kR} \sum_i \tau_t(i) \\ \times \left( \frac{\sqrt{8}}{3} \sqrt{\frac{\omega_{p_{1/2}}}{\omega_{p_{1/2}} + 1}} \Sigma_{1m}^{[\frac{1}{2}]} + 3 \sqrt{\frac{\omega_{p_{3/2}}}{\omega_{p_{3/2}} - 2}} \Sigma_{1m}^{[\frac{1}{2}, \frac{3}{2}]}(i) \right), \\ V_{l=2mt}^\rho(k) = \frac{1}{2f_\rho} \sqrt{\frac{\omega_{p_{3/2}} \omega_s}{(\omega_{p_{3/2}} - 2)(\omega_s - 1)}} \frac{1}{2\pi} \frac{1}{3} \frac{k^2}{\sqrt{\omega_k}} \frac{j_2(kR)}{kR} \\ \times \sum_{i=1}^3 \tau_t(i) \Sigma_{1m}^{[\frac{1}{2}, \frac{3}{2}]}(i).$$

Here

$$\Sigma_{1m}^{[\frac{1}{2}]} = \sum_{m_s m_j} C_{\frac{1}{2} m_j 1 m}^{\frac{1}{2} m_s} |s m_s\rangle \langle p_{1/2} m_j|, \\ \Sigma_{1m}^{[\frac{1}{2}, \frac{3}{2}]} = \sum_{m_s m_j} C_{\frac{3}{2} m_j 1 m}^{\frac{1}{2} m_s} |s m_s\rangle \langle p_{3/2} m_j|, \quad (18)$$

and  $f_\rho$  is the  $\rho$ -meson decay constant with the experimental value 208 MeV.

The peculiar oscillating shape of the CBM form factor has little influence in the case of the  $p$  and  $d$ -wave pions but leads to the unphysical behaviour of the  $s$ -wave scattering amplitude since it crosses zero already at  $W \sim 1950$  MeV. We have cured this problem by replacing  $j_0(kR)$  by an exponential tail for  $k > 1.6/R$  in such a way as not to alter the value of the self energy integral.

## References

1. I.G. Aznauryan et al. (CLAS Collaboration), Phys. Rev. C **80**, 055203 (2009).
2. D. Drechsel, S.S. Kamalov, L. Tiator, Eur. Phys. J. A **34**, 69 (2007).
3. A.V. Anisovich, E. Klempt, V.A. Nikonov, M.A. Matveev, A.V. Sarantsev, and U. Thoma, Eur. Phys. J. A **44**, 203 (2010); see also <http://pwa.hiskp.uni-bonn.de/>.
4. R.A. Arndt, W.J. Briscoe, I.I. Strakovsky, and R.L. Workman, Phys. Rev. C **74**, 045205 (2006).
5. V. Shklyar, H. Lenske, and U. Mosel, Phys. Rev. C **72**, 015210 (2005).
6. R. Shyam and O. Scholten, Phys. Rev. C **78**, 065201 (2008).
7. R. Shyam, O. Scholten, and H. Lenske, Phys. Rev. C **81**, 015204 (2010).
8. F.X. Lee, T. Mart, C. Bennhold, H. Haberzettl, L.E. Wright, Nucl. Phys. A **695**, 237 (2001); see also <http://wwwkph.kph.uni-mainz.de/MAID/kaon/>.
9. M. Batinić, S. Ceci, A. Švarc, and B. Zauner, Phys. Rev. C **82**, 038203 (2010).
10. A.M. Gasparyan, J. Haidenbauer, C. Hanhart, and J. Speth, Phys. Rev. C **68**, 045207 (2003).
11. T.P. Vrana, S.A. Dytman, T.-S.H. Lee, Phys. Rep. **328**, 181 (2000).
12. D.M. Manley, E.M. Saleski, Phys. Rev. D **45**, 4002 (1992) and private communication.
13. A. J. Hey et al. Nucl. Phys. **A362**, 317 (1981).
14. N. Isgur and G. Karl, Phys. Lett. **72B**, 109 (1977).
15. T.A. deGrand, Ann. Phys. **101**, 496 (1976).
16. F. Myhrer and J. Wroldsen, Z. Phys. C **25**, 281 (1984).
17. N. Kaiser, P.B. Siegel, W. Weise, Phys. Lett. **B 362**, 23 (1995).
18. N. Kaiser, T. Waas, W. Weise, Nucl. Phys. **A 612**, 297 (1997).
19. J. Nieves, E. Ruiz Arriola, Phys. Rev. **D 64**, 116008 (2001).
20. T. Inoue, E. Oset, M.J. Vicente Vacas, Phys. Rev. **C 65**, 035204 (2002).
21. C. Garcia-Recio, M.F.M. Lutz, J. Nieves, Phys. Lett. **B 582**, 49 (2004).
22. D. Jido, M. Döring, and E. Oset, Phys. Rev. C **77**, 065207 (2008).
23. B. Juliá-Díaz, B. Saghai, T.-S. Lee, and F. Tabakin, Phys. Rev. C **73**, 055204 (2006).
24. B. Juliá-Díaz, T.S. Lee, A. Matsuyama, T. Sato, Phys. Rev. C **76**, 065201 (2007).
25. J. Durand, B. Juliá-Díaz, T.-S. Lee, B. Saghai, and T. Sato, Phys. Rev. C **78**, 025204 (2008).
26. M. Döring and K. Nakayama, Eur. Phys. J. A **43**, 83 (2010).
27. B. Golli and S. Širca, Eur. Phys. J. A **38**, 271 (2008).
28. B. Golli, S. Širca, and M. Fiolhais, Eur. Phys. J. A **42**, 185 (2009).
29. B. Saghai and Z. Li, Eur. Phys. J. A **11**, 217 (2001).
30. J. He, B. Saghai, Z. Li, Q. Zhao, and J. Durand, Eur. Phys. J. A **35**, 321 (2008).
31. Jun He, B. Saghai, and Z. Li, Phys. Rev. C **78**, 035204 (2008).
32. Jun He and B. Saghai, Phys. Rev. C **80**, 015207 (2009).
33. Jun He and B. Saghai, Phys. Rev. C **82**, 035206 (2010).
34. K. Nakamura et al. (Particle Data Group), J. Phys. G **37**, 075021 (2010).
35. A. Kiswandhi and S. Capstick, Phys. Rev. C **69**, 025205 (2004).
36. W. Deinet et al., Nucl. Phys. B **11**, 495 (1969).
37. W.B. Richards et al., Phys. Rev. D **1**, 10 (1970).
38. R.M. Brown et al., Nucl. Phys. B **153**, 89 (1979).
39. S. Prahkov et al., Phys. Rev. C **72**, 015203 (2005).
40. G. Penner and U. Mosel, Phys. Rev. C **66**, 055211 (2002).
41. L. Tiator, D. Drechsel, S.S. Kamalov and M. Vanderhaeghen, Chinese Physics C **33**, 1069 (2009).
42. V. Mokeev et al. (CLAS Collaboration), in print, Proceedings of the MENU2010 Conference, Williamsburg, May 31-June 4, 2010.
43. [http://gwdac.phys.gwu.edu/analysis/pr\\_analysis.html](http://gwdac.phys.gwu.edu/analysis/pr_analysis.html).
44. A.M. Sandorfi, S. Hoblit, H. Kamano, and T.-S. H. Lee, arXiv:1010.4555v1 [nucl-th].
45. W.T. Chiang, S.N. Yang, L. Tiator, D. Drechsel, Nucl. Phys. A **700**, 429 (2002); see also <http://wwwkph.kph.uni-mainz.de/MAID/eta/etamaid.html>.
46. [http://gwdac.phys.gwu.edu/analysis/pre\\_analysis.html](http://gwdac.phys.gwu.edu/analysis/pre_analysis.html).
47. E. F. McNicoll et al. (Crystal Ball Collaboration at MAMI), Phys. Rev. C **82**, 035208 (2010).
48. [http://gwdac.phys.gwu.edu/analysis/prk\\_analysis.html](http://gwdac.phys.gwu.edu/analysis/prk_analysis.html).
49. W.-M. Yao et al. (Particle Data Group), J. Phys. G **33**, 1 (2006).
50. R.F. Alvarez-Estrada and A.W. Thomas, J. Phys. G: Nucl. Phys. **9**, 161 (1983).